Received: 15 June 2021 | Revised: 23 August 2021 | Accepted: 23 August 2021

DOI: 10.1002/app.51620

ARTICLE

Applied Polymer SCIENCE WILEY

Measurement of effective cure shrinkage of epoxy-based molding compound by fiber Bragg grating sensor using two-stage curing process

Changsu Kim | **Sukrut Prashant Phansalkar** | **Hyun-Seop Lee** | **Bongtae Han**

Mechanical Engineering Department, University of Maryland and College Park, Maryland, USA

Correspondence
Bongtae Han, Mechanical Engineering Department, University of Maryland and College Park, MD 20742, USA.
Email: bthan@umd.edu

Abstract

Cure shrinkage accumulated only after the gel point is known as effective cure shrinkage (ECS), which produces residual stresses inside molded components. The ECS of an epoxy-based molding compound (EMC) is measured by an embedded fiber Bragg grating (FBG) sensor. Under a typical molding condition, a high mold pressure inherently produces large friction between EMC and mold inner surfaces, which hinders EMC from contracting freely during curing. A two-stage curing process is developed to cope with the problem. In the first stage, an FBG sensor is embedded in EMC by a molding process, and the FBG-EMC assembly is separated from the mold at room temperature. The molded specimen is heated to a cure temperature rapidly in the second stage using a constraint-free curing fixture. Several technical issues have to be taken into considerations to ensure that (1) EMC does not pass the gel point before it reaches the cure temperature, and (2) EMC cures uniformly around the FBG during measurements. The ECS of an EMC with a filler content of 88 wt% is measured by the proposed method, and its value is 0.077%. The repeatability of the proposed method is corroborated by the results of a duplicate test.

KEYWORDS

effective cure shrinkage, epoxy molding compound, fiber Bragg grating, gelation, two-stage curing

1 | INTRODUCTION

Epoxy-based molding compounds (EMC) are used widely to house the semiconductor chip and other internal circuitry of electronic packages, in order to provide protections from environments. Such a package is illustrated schematically in Figure 1a, where the encapsulation by EMC is achieved by the well-known transfer molding process. EMC is a composite material consisting of epoxy resin as a matrix and silica particles as a filler. EMC typically has a very large filler content (as high as 90 wt%) to attain desired thermomechanical properties. Figure 1b shows a scanning electron microscopy (SEM) image of EMC, where the high-filler content is evident.

The most widely used molding process for electronic packages, known as *transfer molding*, is illustrated schematically in Figure 2. An EMC pellet is charged in the transfer pot. After heating it to a mold temperature where EMC becomes highly viscous, a ram force is applied to transfer the charge from a transfer pot to cavities containing electronic packages, as shown in (a). The molding compound is driven through narrow channels called "runners," which connect the transfer pot to the gates of cavities. During its transfer, the molding compound remains as a

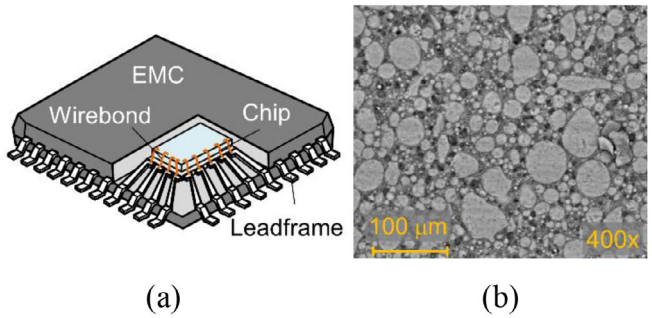

FIGURE 1 (a) Schematic diagram of a semiconductor chip encapsulated by epoxy-based molding compound (EMC), (b) Scanning electron microscopy (SEM) image of typical EMC [Color figure can be viewed at wileyonlinelibrary.com]

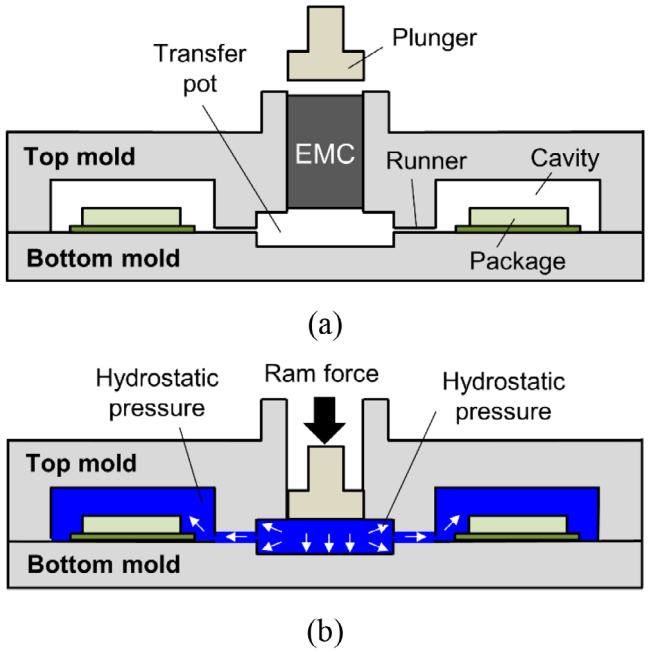

FIGURE 2 Schematic illustration of transfer molding process: (a) Epoxy-based molding compound (EMC) is charged, and the mold is heated to the mold temperature; and (b) Transfer occurs while EMC remains as a viscous liquid [Color figure can be viewed at wileyonlinelibrary.com]

viscous liquid, and thus the mold pressure caused by the ram force is transferred to all cavities, as illustrated in (b). The top mold is separated from the bottom mold for removal of the encapsulated components after curing.

Like other thermosetting polymers, the epoxy resin inside EMC is solidified during a molding process through a chemical reaction that causes polymer chains to cross-link. Each cross-linking causes volumetric shrinkage called "*cure shrinkage*." Cure shrinkage produces curing-induced residual stresses in molded components.[1–3] The polymer's modulus is virtually zero before its gel point, and, thus, only the cure shrinkage accumulated after the gel point, known as the "*effective cure shrinkage* (ECS)",[4] should be used to determine cure-induced residual stresses.

Another critical quantity that affects the magnitude of cure-induced residual stresses is the modulus at a cure temperature. Curing is typically done at a temperature higher than $T_{g\infty}$ (the glass transition temperature of a fully cured polymer), where the modulus rapidly decreases. The modulus of un-filled or lightly filled thermosetting polymers is usually very low at curing temperatures, and thus residual stresses caused by ECS may not be significant. However, the modulus of a highly filled EMC can be as large as 1.5 GPa at a mold temperature, where EMC is transferred and cured.[5] As a result, the residual stresses in molded components, caused by the ECS of EMC, can be very significant at the mold temperature. To the best of authors' knowledge, the ECS of EMC has not been characterized quantitatively because of testing complexity associated with a high mold temperature and a high mold pressure.

Unlike classical methods to measure the *total* cure shrinkage where only a volume change after curing is documented, a technique employed to measure ECS should satisfy two critical requirements: (1) A sensor should be able to measure a stress-induced strain directly during curing since the gel point must be identified accurately; (2) A sensor should be so robust not to be degraded by polymers and/or volatiles as well as harsh curing conditions (temperature, pressure, etc.).

In this study, the ECS value of EMC will be measured by a fiber Bragg grating (FBG) sensor. The FBG is an optical strain sensor that offers very high sensitivity (≈1 microstrain). It is extremely robust, as it is fabricated on a glass fiber. These advantages were exploited to measure the residual stress/strain in composite materials,[6] and the ECS values of various materials.[4,7,8]

For the ECS measurement, an FBG sensor is embedded in a specimen, and thus, a mold to contain uncured polymers in a liquid state is required. The most critical challenge encountered during the measurement is to negate the effect of the mold on the ECS. An extremely soft material was typically used to fabricate the mold to cope with the problem, whereby it deformed together with polymers during curing. As mentioned earlier, however, the EMC molding condition requires the high temperature and pressure, and thus a rigid metal mold must be used to accommodate the condition. Under this condition, large friction between EMC and mold inner surfaces would occur, which would also hinder EMC from contracting freely during curing. In this paper, a novel two-stage curing process is developed to provide a constraint-free curing condition for EMC.

The FBG-based method is reviewed briefly in Section 2. The proposed two-stage curing process is described in

Section 3. Actual measurements of the ECS of an EMC are presented in Section 4. Repeatability of the proposed procedure is discussed in Section 5, and the paper is concluded in Section 6.

2 | FBG-BASED METHOD TO MEASURE ECS

The definition of the ECS is reviewed first. The fundamentals of the FBG-based method to measure the ECS are followed.

2.1 | Effective cure shrinkage

The behavior of a typical polymer system during curing is illustrated in Figure 3.[8] where the x-axis shows an arbitrary time scale, and the y-axis represents two polymer properties associated with curing (cure shrinkage, $\varepsilon(t)$ and modulus, $E(t)$), normalized by their final values, ε_∞ and E_∞, obtained at full-cure.[9] The cure shrinkage is proportional to the extent of cure, and the modulus evolves non-linearly with time.

As mentioned earlier, cure shrinkage does occur before the gel point (denoted as t_{gel}), but the modulus associated with the cure shrinkage developed before t_{gel} is virtually "zero." In the figure, the time after t_{gel} and the ECS are denoted as $\tilde{t}$ and $\tilde{\varepsilon}(\tilde{t})$, respectively. It is important to note that the moment at which gelation occurs must be precisely identified in order to measure the ECS quantity accurately.

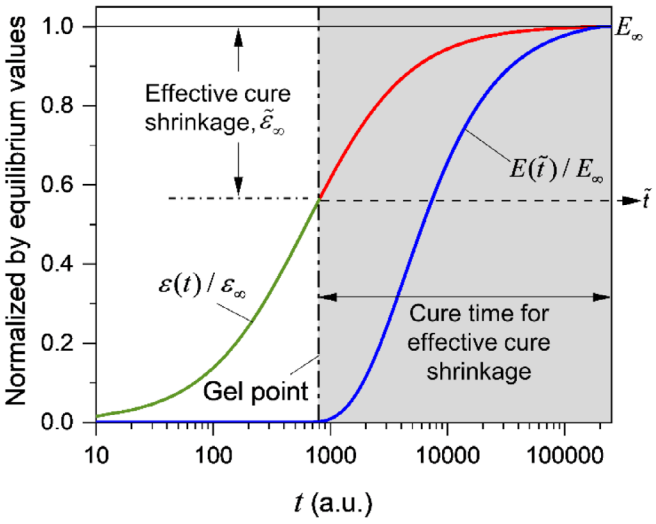

FIGURE 3 Schematic illustration of cure shrinkage and modulus evolution during curing [Color figure can be viewed at wileyonlinelibrary.com]

2.2 | FBG-based method

A FBG reflects a narrow band of wavelengths of light while transmitting other wavelengths. It is achieved by creating a periodic variation in the refractive index of an optical fiber.[10] The center of the reflected wavelength is called Bragg wavelength (BW), which is defined as:

$$\lambda_B = 2n_{eff}\Lambda, \tag{1}$$

where λB is BW; n_{eff} is the effective refractive index; and Λ is the grating pitch.

In the method, an FBG sensor is embedded in a cylindrically shaped uncured polymer. As illustrated in Figure 4, the polymer shrinks around the FBG sensor as curing progresses. After the gel point, the ECS of the polymer starts to deform the FBG sensor, and the BW shift is resulted.

The generalized plane strain solution for the stress components of the FBG sensor, caused by the ECS, was first derived by Wang et al.[11] It was later utilized to define the relationship between the BW shifts and the ECS.[4,8,9] The relationship can take a form of

$$\tilde{\varepsilon}_\infty = \frac{\Delta\lambda_B}{\lambda_B}\left[F\left(E_f, E_p, \beta\right)\right]^{-1}, \tag{2}$$

where $\tilde{\varepsilon}_\infty$ is the linear ECS; $\Delta\lambda_B$ is the BW shift measured during curing; E_f and E_p are the moduli of the fiber and the polymer, respectively; $\beta = \frac{r_p}{r_f}$ is called "configuration", where r_f and r_p are the radii of the fiber and the polymer, respectively; and $F()$ is a nonlinear function, which can be expressed explicitly. The ECS can be determined from $\Delta\lambda_B$ when the Poisson's ratio and the modulus of the polymer are known.[8,9]

It was also shown in Ref. [11] that the curing-induced radial stress of the fiber is much smaller than the corresponding axial stress, which makes the loading

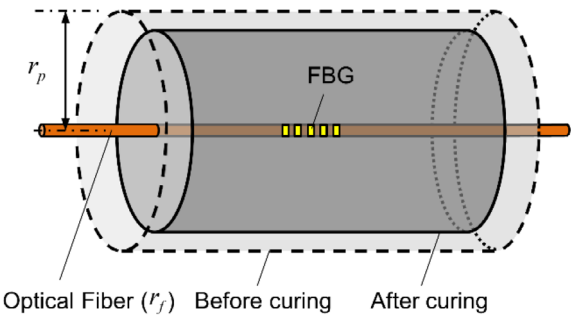

FIGURE 4 Schematic illustration of a specimen configuration with an embedded FBG sensor [Color figure can be viewed at wileyonlinelibrary.com]

condition of the FBG sensor virtually uniaxial. Under this condition, Equation (2) is reduced to[11]:

$$\tilde{\varepsilon}_{\infty} = \frac{\Delta\lambda_B}{\lambda_B(1-P_k)} \cdot \zeta(E_p, \beta), \tag{3}$$

where P_k is the equivalent strain-optic constant,[10] and ζ is the strain-transfer ratio, which is defined as $\frac{\varepsilon_f}{\tilde{\varepsilon}_{\infty}}$ where ε_f is the axial strain of the fiber caused by the ECS.

The strain-transfer ratio is strongly dependent on the volume stiffness ratio between the polymer and the fiber. The volume stiffness ratio, $\widehat{R}_{VS}$, can be defined as[12]:

$$\widehat{R}_{VS} = \frac{E_p\left(r_p^2 - r_f^2\right)}{E_f \cdot r_f^2}, \tag{4}$$

The value of ζ converges to "unity" when the volume stiffness ratio approaches a large value. Under this condition (defined as "infinite configuration" in Ref. [12]), the ECS of a polymer is fully transferred to the fiber regardless of the polymer's modulus.

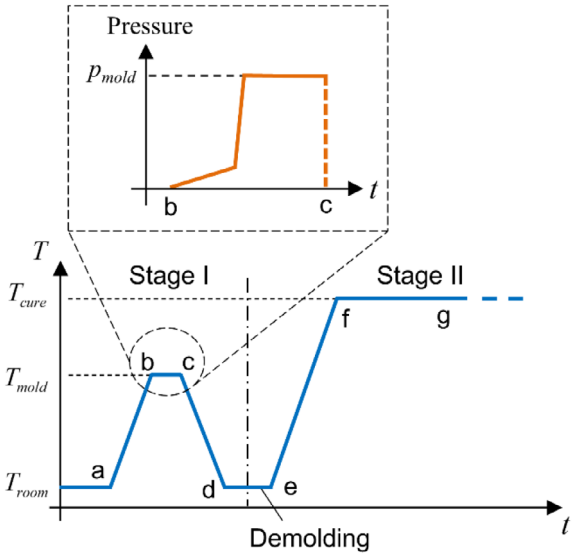

FIGURE 5 Schematic illustration of two-stage curing process. Stage I: (a, b) Heating to T_{mold}; (b) Pressure application; (c) Removal of pressure and cooling down to T_{room}; and (d) Demolding at T_{room}. Stage II: (e - f) Heating to T_{cure}; (f - g) Temperature stabilization at T_{cure}; and (g) Curing [Color figure can be viewed at wileyonlinelibrary.com]

3 | TWO-STAGE CURING FOR CONSTRAINT-FREE MEASUREMENT

A two-stage curing process is developed to cope with the problem associated with friction caused by the mold pressure. A constraint-free cure condition is described first. Criteria to determine a specimen configuration and a cure temperature (T_{cure}) are followed.

3.1 | Two-stage curing process

A history of temperature and pressure during the proposed two-stage curing process is illustrated in Figure 5. Prior to Stage I, a small hole (slightly larger than the fiber diameter) is drilled along the center of a preformed EMC pellet to accommodate the optical fiber. In Stage I, the EMC and FBG subassembly is heated slowly to a mold temperature, T_{mold}, (a - b), and a mold pressure is applied at T_{mold} (b). After the pellet is collapsed into a metal mold (b), the mold pressure is removed at (c), and the mold is cooled down to room temperature (d). The molded EMC specimen with the embedded fiber is separated from the mold at room temperature (d - e).

The inset of Figure 5 shows how the pressure is applied at T_{mold}. It is suggested that a small amount of pressure be applied slowly first to collapse the pellet, and then the rest of mold pressure (p_{mold}) be applied quickly. This procedure of pressure application minimizes the lateral movement of the fiber while collapsing the pellet. It is important to note that T_{mold} should be only slightly higher than T_g of the uncured EMC so that the pellet can deform under the mold pressure while minimizing the amount of curing.

In Stage II, the EMC specimen prepared in Stage I is heated to a cure temperature, T_{cure} (e - f), and is continuously cured until no change in the BW shift is observed (g). The most critical requirement for Stage II is that the EMC specimen should not reach its gel point before the specimen reaches T_{cure}. (f). It is to be noted that the BW change at a constant temperature occurs only when a fiber is subjected to a mechanical strain. This critical feature is to be exploited to identify the gel point during curing (f - g).

Several technical considerations are to be given to determine a proper specimen configuration, β, and a cure temperature, T_{cure}. The configuration will have to be determined first. It is clear from Equation (4) that the volume stiffness ratio, $\widehat{R}_{VS}$, and thus the strain transfer ratio, ζ, increases as the EMC radius (i.e., β) does. However, the maximum configuration is limited in practice due to heat generation during curing. If heat generation produces a large temperature gradient within a specimen, the accuracy of ECS measurement can be affected significantly.[9] In general, the requirement of the infinite configuration sets the lower bound of β while a condition for uniform curing does the upper bound.

As mentioned earlier, the value of T_{cure} should be chosen carefully so that that the EMC specimen at T_{cure} does not pass the gel point. This sets the maximum value of T_{cure}. The minimum value of T_{cure} should be greater than $T_{g\infty}$ (the glass transition temperature of a fully cured EMC). It is well known that T_g of polymer increases as the extent of cure increases. If T_{cure} is lower than $T_{g\infty}$, a phenomenon known as vitrification will occur when the glass transition temperature of a partially cured EMC reaches T_{cure}.[13,14]

4 | MEASUREMENTS AND RESULTS

An EMC with a filler content of 88 wt% was tested. The specimen configuration and the T_{cure} are determined first. The experimental setup for the two-stage curing is described, and the measurement of the ECS is presented.

4.1 | Specimen configuration and cure temperature

The lower bound of the configuration was estimated first by considering the strain-transfer ratio, ζ. The E and β combinations that offer the infinite configuration (i.e., $\zeta > 0.99$) are shown in Figure 6 (green solid line). The temperature-dependent moduli reported in Ref. [5] were used to calculate the corresponding E and T combinations that provide the lower bound. The results are also shown in Figure 6 (blue solid circles).

For the upper bound of the configuration, a combined analysis of cure kinetics and heat generation should be conducted to estimate the extent of cure distribution within the specimen. Let us consider the well-known n^{th} order cure kinetics model, which is expressed as:

$$\frac{dp}{dt} = k_T(1-p)^n, \tag{5}$$

where p and n are the extent of cure and the reaction order, respectively; k_T is a temperature-dependent rate constant, which can be defined by the Arrhenius relationship. The governing equation based on the n^{th} order model that describes a temperature distribution during curing can be expressed as[9]:

$$\frac{K}{\rho}\left(\frac{\partial^2 T}{\partial r^2} + \frac{1}{r}\frac{\partial T}{\partial r}\right) + k_T(1-p)^n \Delta H = c_p \frac{\partial T}{\partial t}, \tag{6}$$

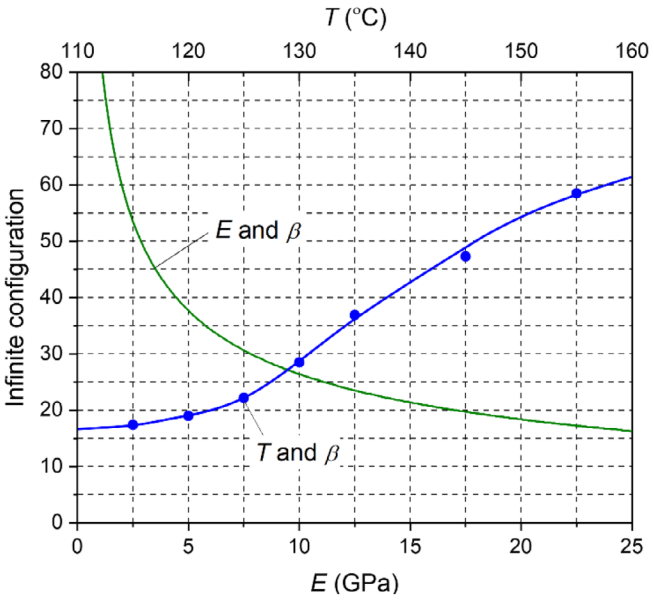

FIGURE 6 E and β combinations required for the infinite configuration (green line); blue solid circles (E and T combinations) are obtained from temperature-dependent moduli [Color figure can be viewed at wileyonlinelibrary.com]

where K, ρ, c_p and ΔH are the thermal conductivity, the density, the specific heat, and the total exothermic heat, respectively.

The iterative numerical approach developed in Ref. [9] was utilized in this study. In the approach, the temperature distribution within a small time step is calculated first through a transient thermal analysis, where a uniform heat generation caused by exothermic curing process is used as an input thermal loading. The resultant non-uniform temperature distribution is subsequently used to determine the extent of cure of the next time step using the cure kinetics model. The procedure is iterated until all part of specimen reaches the complete cure status (i.e., $p = 1$). The evolutions of temperature distribution and extent of cure obtained by recording the intermediate results during curing.

The analysis was conducted using the properties reported in Ref. [15] ($\Delta H = 18.0$ J/g; $n = 0.93$; $k_T = 10^{-3}$/s). Representative distributions of temperature and extent of cure for $\beta = 90$ are illustrated in Figure 7, where $T = 130$°C and $t = 478$ s. The values of $\Delta p_{\max}$ ($= p_{\text{in}} - p_{\text{out}}$) at various temperatures were calculated as a function of β, where p_{in} and p_{out} are the values of cure extent at the center and the surface of a specimne, respectively. The results are shown in Figure 8. It is to be noted that the green solid circle indicates the condition used for the results in Figure 7. The horizontal line defines the acceptable criterion for Δp_{max} ($= 1\%$).[9] The intersections points (red solid circles) indicate the largest

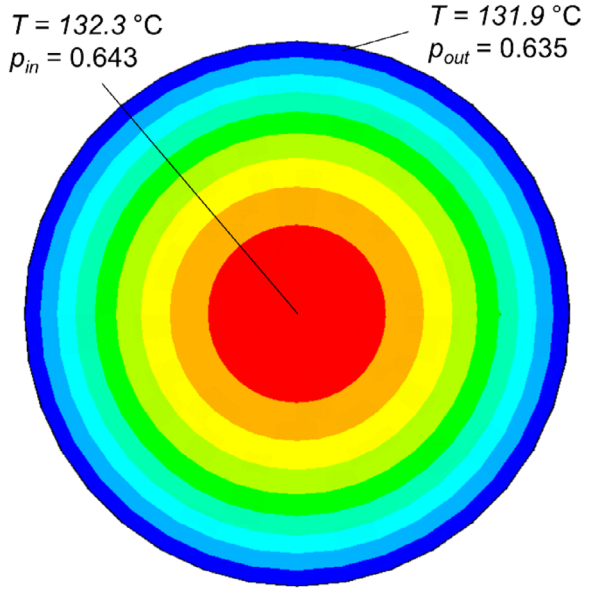

FIGURE 7 Representative results for $\beta = 90$, obtained from the combined cure kinetics and heat generation analysis: The distributions of the temperature and extent of cure at $t = 478$ sec for $T_{cure} = 130°C$ [Color figure can be viewed at wileyonlinelibrary.com]

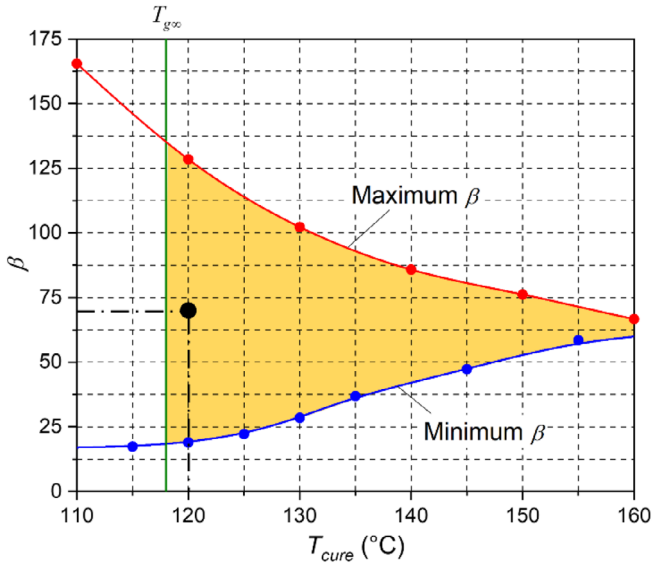

FIGURE 9 Acceptable range for the proposed procedure (yellow shaded area), where the solid black circle indicates the values of configuration, and T_{cure} used for the study: $\beta = 70$ and $T_{cure} = 120°C$ [Color figure can be viewed at wileyonlinelibrary.com]

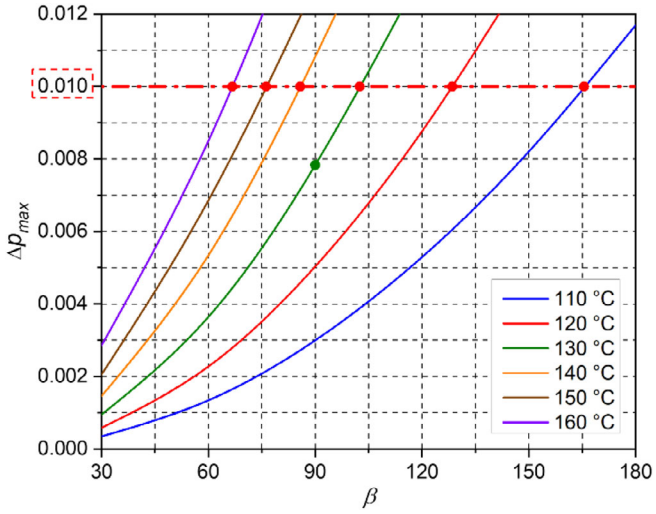

FIGURE 8 Maximum difference of extent of cure as a function of configuration, where the horizontal line shows the criterion for Δp_{max} used in the study [Color figure can be viewed at wileyonlinelibrary.com]

configuration allowed at each temperature, which are plotted as a function of temperature in in Figure 9 (solid red circles).

The value of $T_{g\infty}$ is required to set the low bound of T_{cure}. It was measured by a dynamic mechanical analyzer (RSA3, TA Instruments). The value is shown as a vertical line (118°C) in Figure 9 together with the lower bound (blue solid dots in Figure 6). The shaded area in Figure 9 represents the acceptable range.

The value of β was chosen in the middle of the range considering the uncertainties of the properties used in the analyses. The value of T_{cure} was chosen at the lower side of the range to ensure that the specimen does not pass the gel point in Stage II. The solid black circle in Figure 9 indicates the values of configuration and T_{cure} used for the study: $\beta = 70$ and $T_{cure} = 120°C$.

4.2 | Testing and results

A procedure developed in Ref. [5] was used to fabricate an EMC specimen with an embedded FBG during Stage I. The experimental setup is shown schematically in Figure 10. A metal mold is attached to a hot plate (HCP306S: Instec) for temperature control. An EMC pellet is placed inside the mold (diameter = 8.8 mm and length = 15 mm). The pressure regulator (ER3000: Tescom) provides air pressure to a pneumatic piston (121-DV: BIMBA). The piston force is transferred to a mechanical plunger that provides the required mold pressure (7 MPa), as shown in the inset. The maximum pressure of the compressed air line is only 0.69 MPa, but the required mechanical pressure is achieved by the pneumatic piston that has a diameter much larger than the

plunger diameter. More details about the pressure application can be found in Ref. [5].

The optical fiber (diameter = 125 μm) is inserted through a small through hole drilled in the center of the EMC pellet. As shown in the inset, the fiber position is adjusted in such a way that the Bragg grating (5 mm long) is located in the middle of pellet. The BW is documented by an FBG interrogator (si155: Micron Optics). To prevent leakage of EMC during pressure application, a silicone rubber pad is placed between the plunger head and the specimen. The mold is covered with an insulation box (not shown) before heating.

A pretension was applied to the fiber to make the fiber remain straight during Stage I. Two fiber clamps were used to apply a desired pretension. Clamp 1 was fixed to the bottom support, but the position of Clamp 2 was made adjustable using an adjusting screw to control the pretension amount, as illustrated in the second inset. A pretension of 3000 microstrain with an increment of approximately 100 microstrain was readily achieved.

Preliminary tests were conducted to determine the lowest T_{mold} while monitoring the plunger movement. The EMC pellet was collapsed without voids at 90°C, and it was selected as T_{mold}. In Stage I, the pressure to the plunger was increased slowly to 0.5 MPa for the first 15 s, and it was quickly increased to 7 MPa for the next 5 s. The actual pressure applications used in Stage I are shown in Figure 11.

The setup was cooled down to room temperature slowly after the pressure was removed. The EMC

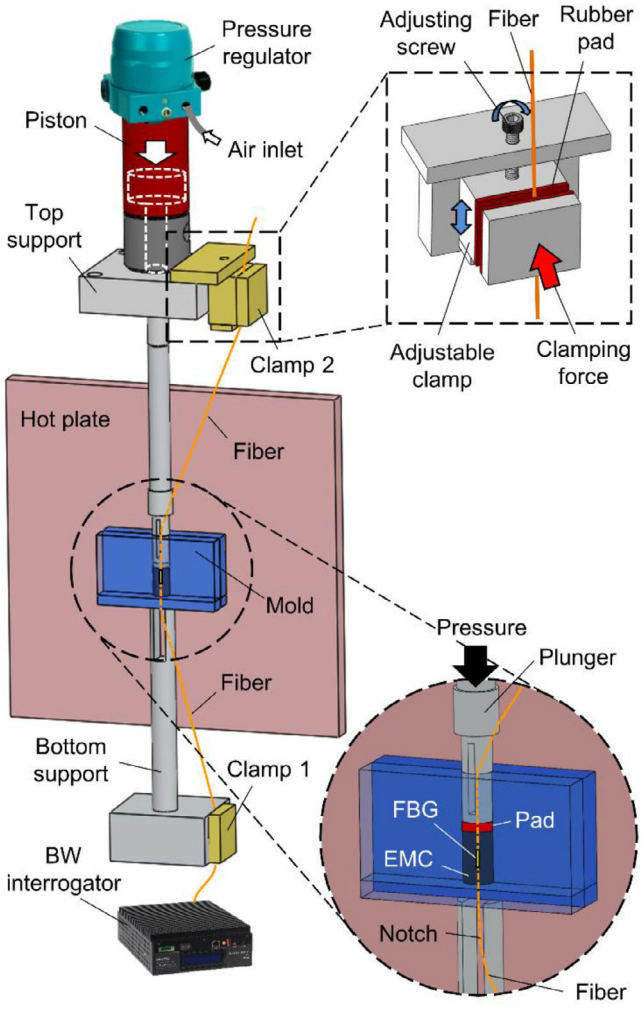

FIGURE 10 Schematic diagram of the setup used for Stage I, where the insets show the detailed view of the custom-designed mold and Clamp 2 [Color figure can be viewed at wileyonlinelibrary.com]

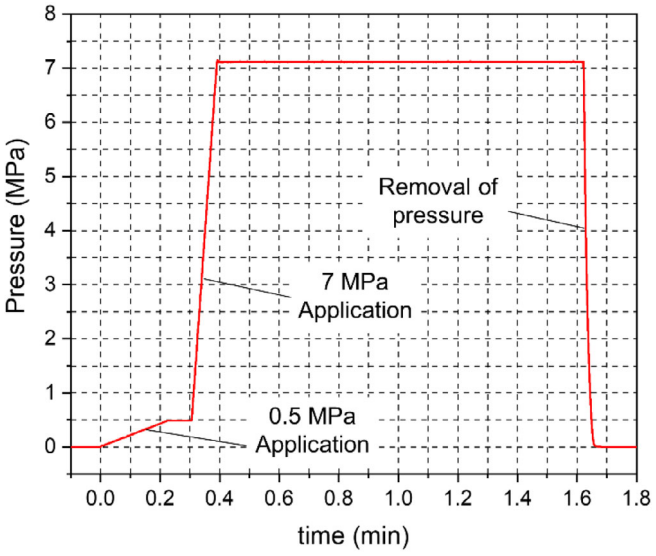

FIGURE 11 History of pressure application in stage I [Color figure can be viewed at wileyonlinelibrary.com]

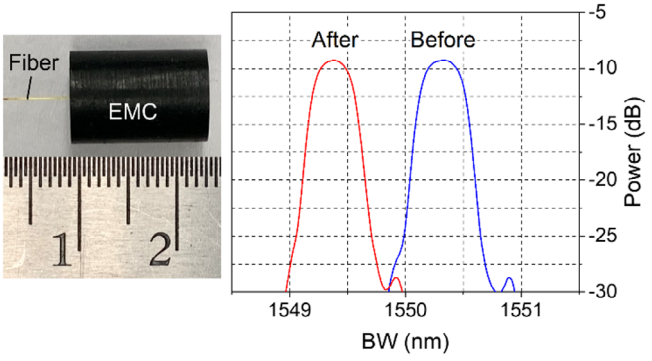

FIGURE 12 Molded specimen obtained after Stage I and reflection spectra of FBG before and after Stage I [Color figure can be viewed at wileyonlinelibrary.com]

specimen was separated from the mold. The molded specimen after separation is shown in Figure 12. The reflection spectra of the FBG before and after Stage I were measured to ensure the uniformity of the molded specimen. The results are also shown in Figure 12. The spectra are nearly identical, which confirms that the specimen molded uniformly during Stage I.

The setup used for Stage II is shown schematically in Figure 13a. A metal fixture that had a hole slightly larger than the molded specimen was placed in a microprocessor-controlled convection oven (EC11A: Sun Electronic Systems). The convection oven was preheated to T_{cure} (120°C). Then, the specimen was inserted in the preheated fixture through a small hole built on a sidewall of the oven. A silicone plug is used to block the hole while passing the fiber. This procedure minimized disturbance of the thermal equilibrium of the oven. The BW was recorded continuously during Stage II.

The performance of the setup was evaluated using an auxiliary specimen with a thermocouple embedded at the center. The temperature history of the thermocouple specimen after placed inside the fixture ($t = 0$) to of Figure 13b. The temperature increased rapidly and became stable at T_{cure} within 3 min.

The complete BW history obtained during Stage II is shown in Figure 14. The inset shows the BW during initial 40 min. As expected from the temperature data of Figure 13b, the BW increased rapidly during heating, and then became stable at T_{cure}. The BW remained constant for approximately 12 min (a plateau region), and began to decrease. The result confirms that the molded specimen did not pass the gel point of EMC before its temperature became stable at T_{cure}. The end of the plateau region was determined as the gel point.

The total BW shift was determined from Figure 14, and it was 936 pm. The total ECS, $\tilde{\varepsilon}_{\infty}$, was calculated from the BW shift using Equation (3), and it was 0.077%. This is approximately 43% of the mold shrinkage value provided by the EMC manufacturer. The relationship between the ECS and the mold shrinkage can be found in.[16]

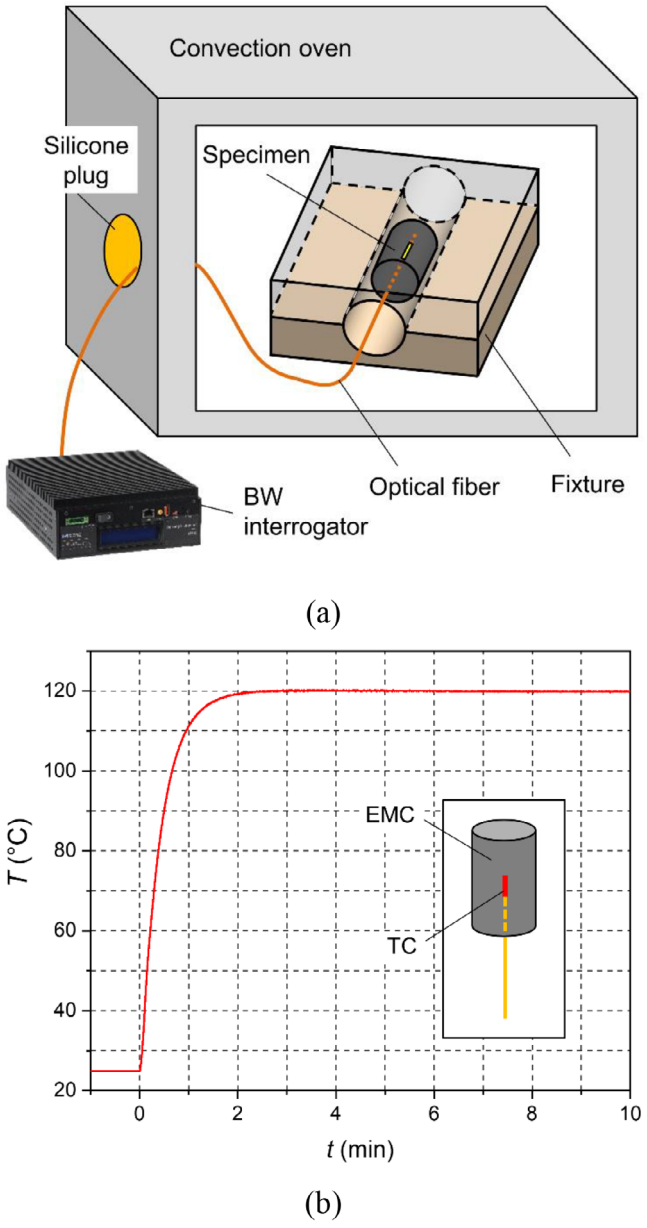

FIGURE 13 (a) Schematic diagram of a setup for Stage II and (b) The temperature history of a specimen for the first 10 min of Stage II, where the x-axis represents elapsed time after the specimen is placed inside the fixture ($t = 0$) [Color figure can be viewed at wileyonlinelibrary.com]

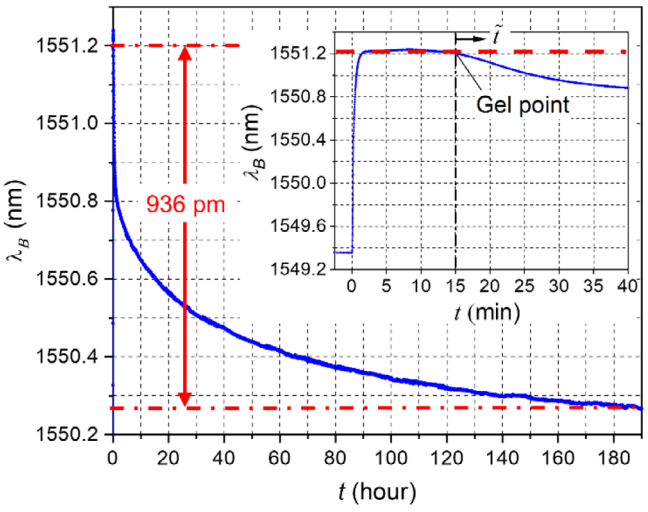

FIGURE 14 BW obtained during Stage II where the inset shows the results of initial 40 min [Color figure can be viewed at wileyonlinelibrary.com]

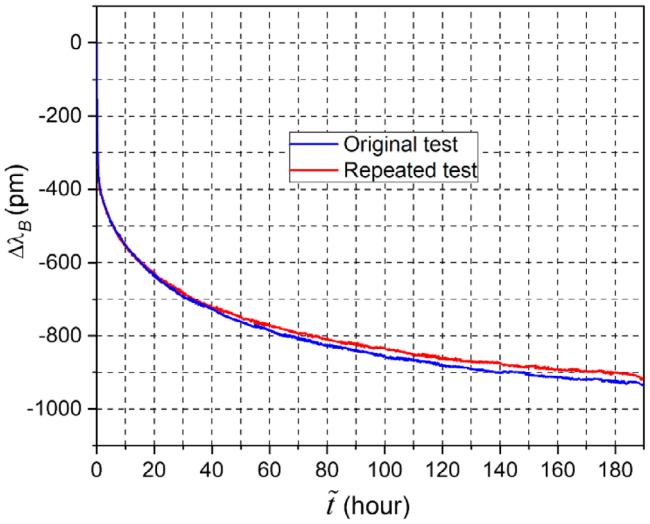

FIGURE 15 BW changes obtained from the original test are compared with the repeated test [Color figure can be viewed at wileyonlinelibrary.com]

5 | DISCUSSION

The measurement procedure implemented in the study was repeated to investigate its repeatability. The results obtained from the second test during Stage II are compared with the original test results (Figure 14) in Figure 15, where the Bragg wavelength changes ($\Delta\lambda_B$) after the gel point were calculated for direct comparison. It is clear from the comparison that the time-dependent histories of Bragg wavelength (λ_B) are virtually identical. The total Bragg wavelength changes of the two tests are 936 and 916 pm, which correspond to the ECS values of 0.077% and 0.075%, respectively. In spite of the complexity involved in the testing procedure, including the high pressure application, the ECS values obtained from two completely independent measurements differ only by 2%. The gel point detected from both tests were also very close (≈ 15 min), which was another indication that the measurement procedure was repeatable.

During the transfer molding processes described in Figure 2, the molding compound cures rapidly at the mold temperature, and quickly passes its gel point (typically within a couple of minutes). As mentioned earlier, the molding compound becomes a deformable solid at the gel point. After the gel point, the pressure to fill the cavities is no longer transferred to the molding compound inside the cavities, although the pressure is maintained; that is, the mold pressure deforms only the molding compound near the transfer pot (yellow area). This is illustrated schematically in Figure 16. This provides the technical rationale for the reason why the ECS must be measured after the mold pressure is removed for the prediction of residual stresses produced by the transfer molding process.

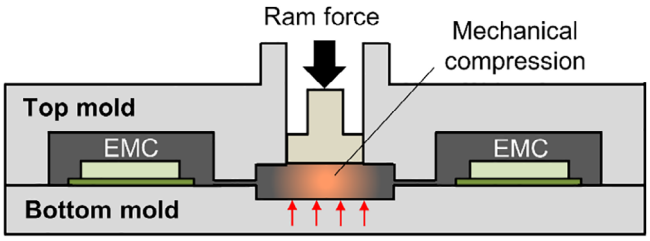

FIGURE 16 Schematic illustration of stresses on epoxy-based molding compound (EMC) immediately after EMC passes its gel point [Color figure can be viewed at wileyonlinelibrary.com]

6 | CONCLUSION

An FBG sensor was employed to measure the ECS of EMC. A two-stage curing process was developed to cope with technical challenges associated with the transfer mold process, in particular the high mold pressure. The ECS was measured under the friction-free condition by the proposed procedure while clearly identifying the gel point. The results from the repeated test confirmed the measurement repeatability of the proposed method.

The ECS of the EMC tested in the current study is 0.077%, which is much smaller than the shrinkage values reported in the literature. It is also significantly different from the mold shrinkage value that EMC manufactures typically provide. It is expected that the ECS of other EMC's with a similar filler content would be comparable.

ORCID

Bongtae Han https://orcid.org/0000-0003-3721-9738

REFERENCES

[1] J. Lange, S. Toll, J.-A. E. Månson, A. Hult, *Polymer* **1995**, *36*, 3135.
[2] D. B. Adolf, J. E. Martin, R. S. Chambers, S. N. Burchett, T. R. Guess, *J. Mater. Res.* **1998**, *13*, 530.
[3] M.-L. Sham, J.-K. Kim, *Compos. Part A* **2004**, *35*, 537.
[4] Y. Sun, B. Han, E. Parsa, A. Dasgupta, *J. Mater. Sci.* **2014**, *49*, 8301.
[5] Y. Sun, H.-S. Lee, B. Han, *Exp. Mech.* **2017**, *57*, 313.
[6] D. Kinet, P. Mégret, K. W. Goossen, L. Qiu, D. Heider, C. Caucheteur, *Sensors* **2014**, *14*, 7394.
[7] Y. Du, J.-H. Zhao, P. Ho, *J. Electron. Packag.* **2001**, *123*, 196.
[8] S. P. Phansalkar, C. Kim, B. Han, P. J. Gromala, *J. Mater. Sci.* **2020**, *55*, 9655.
[9] Y. Wang, L. Woodworth, B. Han, *Exp. Mech.* **2011**, *51*, 1155.
[10] K. O. Hill, G. Meltz, *J. Lightwave Technol.* **1997**, *15*, 1263.
[11] Y. Wang, B. Han, D. Kim, A. Bar-Cohen, P. Joseph, *Exp. Mech.* **2008**, *48*, 107.

[12] Y. Sun, Y. Wang, Y. Kim, B. Han, *Exp. Mech.* **2014**, *54*, 593.
[13] G. Wisanrakkit, J. Gillham, *J. Appl. Polym. Sci.* **1990**, *41*, 2885.
[14] J. Schawe, *Thermochim. Acta* **2002**, *388*, 299.
[15] D. E. Lee, H. W. Kim, B. S. Kong, H. O. Choi, *J. Appl. Polym. Sci.* **2017**, *134*, 45252.
[16] C. Kim, S. P. Phansalkar, H.-S. Lee, B. Han, presented at 2019 *IEEE 69th ECTC*, Las Vegas, NV, May **2019**.

How to cite this article: C. Kim, S. P. Phansalkar, H.-S. Lee, B. Han, *J. Appl. Polym. Sci.* **2021**, e51620. https://doi.org/10.1002/app.51620